

<https://doi.org/10.1038/s40494-025-02271-z>

'Three strong and three weak' seismic-resistant wisdom of ancient Chinese wooden structures

Check for updates

Chengya Zhang¹, Xianjie Meng²✉, Yue Wang¹, Zhirong Jia¹ & Saiqin Wu¹

Ancient Chinese wooden structures exhibit remarkable organic characteristics, reflected in their highly integrated construction and exceptional seismic performance. To explore the seismic-resistant wisdom inherent in ancient wooden structures, this study provided an in-depth interpretation of traditional construction techniques and carried out quasi-static and dynamic tests on two timber structure models designed with characteristic Song dynasty architectural features. The structural characteristics of key joints and their deformation behavior were clarified, the energy dissipation mechanism and its correlation with seismic performance were analyzed, and the stiffness differences among various structural layers and their collaborative seismic-resisting mechanism were revealed. The results demonstrate that the ancient wooden structures possess the advantages of “weak connections yet strong deformability,” “weak energy dissipation yet strong seismic resistance,” and “weak resonance yet strong synergy.” These findings systematically reveal the seismic mechanisms of ancient wooden structures and offer valuable insights for the seismic design and improvement of modern buildings.

Ancient Chinese wooden structures are distinctive for their magnificent appearance, exquisite details, convenient assembly, and excellent earthquake resistance. Wooden structures entered a period of refinement in the Tang Dynasty¹ and maturity in the Song Dynasty with the compilation of the *Yingzao Fashi*², which systematically elaborated on the design and construction of official architecture in the Song Dynasty and featured several high-grade, meticulously constructed wooden buildings³. The maturity of Song Dynasty wooden structures is reflected in standardized and modularized construction^{4–6}, rigorous and scientific framing⁷, flexible and diverse forms⁸, achieving an organic unity between architectural construction and structural performance^{9,10}.

Ancient wooden structures are divided from bottom to top into the column frame, Dou-gong, and roof layers (Fig. 1b). Column bases typically use three connection methods: flat floating, Guan-jiao tenon, and Tao-ding tenon^{11–13}. Flat floating column bases rest on plinths, constrained only by the friction between the columns and plinths¹⁴, making it the most common column base connection. Guan-jiao tenon features a mortise in the center of the plinth, connecting to the column via a wooden pin. Guan-jiao tenon is similar but with a through-mortise in the plinth and a larger mortise size¹⁵. Column-head mortise-tenon joints commonly use straight^{16,17}, dovetail, and hoop tenons¹⁸. Straight tenons include through tenons and half tenons^{19,20}. Dou-gong consists of multiple Dou and Gong components connected layer

by layer via mortise-tenon joints, connecting columns to Lu-dou through An-xiao, and linking columns, beams, and Dou-gong via longitudinal and horizontal components^{21–23}. The positions and methods of each connection node are illustrated in Fig. 1a.

Ancient wooden structures exhibit excellent seismic performance, with structural mechanical characteristics and seismic properties showing both commonalities and differences owing to the varying connection methods. The hysteretic curves of the three column-base connections under horizontal cyclic loading all exhibited an “S” shape²⁴. Among them, the Tao-ding tenon has the highest lateral stiffness¹⁵, whereas flat floating has the plump hysteretic curves, with an energy dissipation capacity approximately 1.28 times that of the Guan-jiao tenon and 1.50 times that of the Tao-ding tenon, indicating that flat floating facilitates energy dissipation through frictional sliding during earthquakes. The columns exhibited swaying characteristics and good deformation recovery under horizontal cyclic loading, with an “S”-shaped hysteretic curve. Even under ultimate loads, no significant damage occurred to the column components, indicating that column rocking resulted in weak energy dissipation but strong deformability of the column frame layer²⁵. These characteristics differ from those of column-head mortise-tenon joints and Dou-gong nodes²⁶. Column-head mortise-tenon joints exhibited an inverted “Z”-shaped hysteretic curve with significant pinching, accompanied by joint slippage and shear deformation.

¹College of Architecture and Art, Taiyuan University of Technology, Taiyuan, China. ²College of Civil Engineering, Taiyuan University of Technology, Taiyuan, China.

✉ e-mail: mengxianjie01@tyut.edu.cn

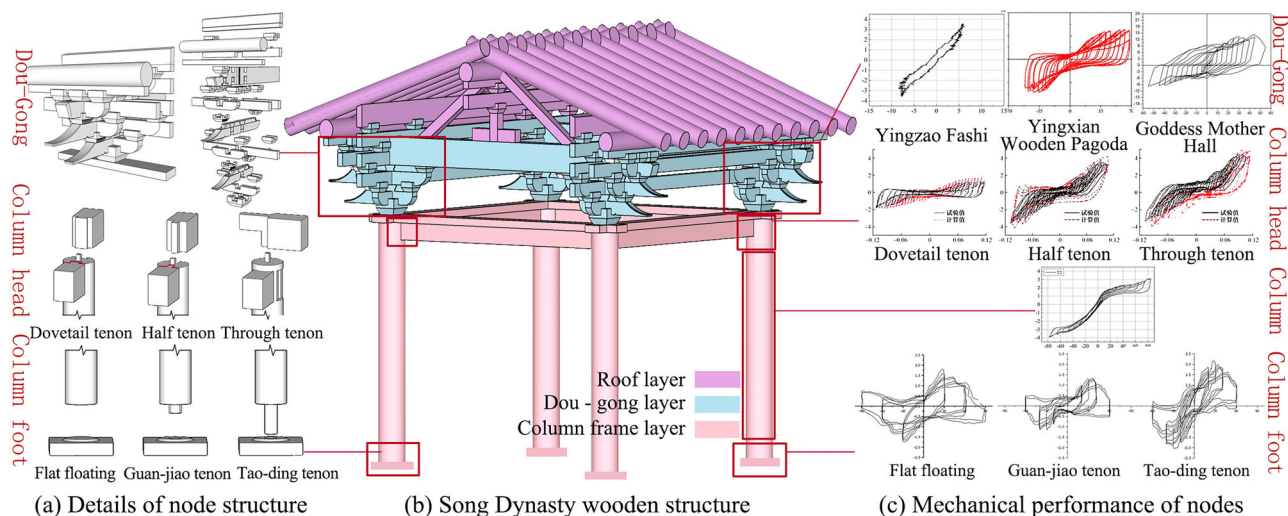


Fig. 1 | Basic structural characteristics of ancient buildings. a Details of node structure; **b** Song Dynasty wooden structure; **c** Mechanical performance of nodes^{15,28,56,57}.

Among these, dovetail tenons have the plumpest hysteretic curves, with the strongest plastic deformation and energy dissipation capacity, whereas half tenons perform the worst²⁷. The deformation and relative displacement between tenons and mortises are key to vibration reduction and energy dissipation in wooden structures^{28,29}. Dou-gong nodes show a plump bow-shaped hysteretic curve under horizontal cyclic loading, indicating good energy dissipation performance⁶. Additionally, Dou-gong has a much higher stiffness than the column frame layer³⁰, with energy dissipation achieved through sliding friction between the components³¹ and the plastic deformation of the lower components. The mechanical performance of each connection component is illustrated in Fig. 1c.

Song Dynasty wooden structures, representative of the mature period of ancient architecture, combine excellent seismic performance with harmonious and unique architectural aesthetics. Their complex configurations, diverse connection methods, and distinct seismic properties^{32,33} achieve an organic unity between structural rationality and construction methods through synergistic work³⁴, reflecting craftsmen ingenious design for balance in Chinese wooden architecture^{35,36}. However, existing research focuses on the mechanical properties and construction of wooden structures separately, lacking a scientific exploration of the organic concept combines the two. Thus, quantifying and verifying the seismic advantages of Song Dynasty wooden structures through modern experimental methods and establishing scientific correlations between seismic performance and architectural configurations not only sheds light on Song Dynasty architectural technology but also provides a basis for improving modern building seismic performance^{37,38}, promoting the inheritance and application of excellent traditional culture.

Methods

Research object

Model testing serves as one of the important methods for studying the seismic performance of ancient wooden structures. To more scientifically elucidate the seismic resilience of these structures, this study conducted both static and dynamic tests on two representative wooden structural models. One model (M1) was constructed at a 1:2 scale based on the 7th-class timber frame described in Yingzao Fashi—the Song Dynasty architectural standard for wooden structures (Fig. 2). The other model (M2) was designed at a 1:3 scale, replicating the front-eave central beam frame of the first story of the Goddess Mother Hall, a typical example of existing Song-style wooden architecture in China. In both models, the columns are simply placed on the foundation without any fixed connections at the base. The components are connected using traditional techniques: Lan-e and columns are joined by dovetail tenons, Pu-pai-fang are mounted on top of the columns, and Dou-gong are installed on the Pu-pai-fang. These elements are further secured

using An-xiao. Compared to M1, model M2 incorporates an additional sloped roof structure, as illustrated in Fig. 3. M1 uses camphor pine as the model material. M2 uses larch as the model material, and the material properties parameters are determined through material testing, as shown in Table 1.

Research methodology

Quasi-static test T1 and shaking table test T2 were conducted on model M1, while quasi-static test T3 and shaking table test T4 were conducted on model M2. The loading devices for T1 and T3 are shown in Fig. 4; those for T2 and T4 are shown in Fig. 5, and the measurement devices are shown in Fig. 6. For all four tests, westward loading was defined as positive, and eastward loading as negative.

The vertical loads for the models were determined by referencing the roof loads of similarly sized ancient buildings³⁹ and scaling down calculations⁴⁰, resulting in 45kN for M1 and 54kN for M2. For M1, a vertical load in T1 was applied via three layers of concrete slabs totaling 45kN on the Dou-gong, whereas T2 used 50 steel blocks (2200 × 40 × 20 mm) totaling 45kN. For M2, T3, and T4 used three layers of 60 steel blocks totaling 54kN. Both the concrete slabs and steel blocks can be regarded as non-deformable rigid bodies, consistent with the assumption that the roofs of ancient wooden structures behave as a rigid whole.

The horizontal ultimate displacement of four-column wooden structures is approximately equal to the column radius⁴¹. With a column radius of 97 mm for M1 and 89 mm for M2, the estimated ultimate displacements were 90–100 mm for T1 and 80–90 mm for T3. The tests used 8 levels of cyclic loading, with horizontal displacement amplitudes of 10 mm, 20 mm, and so on, up to the ultimate state (Max). The horizontal cyclic loading time-history curves for T1 and T3 are shown in Fig. 7.

T2 and T4 shaking table tests used sinusoidal excitation with a vibration amplitude of 6 mm. The shaking table was driven by a 30 kW servo motor, with the motor speed gradually increasing from 0 r/min to 300 r/min and then decreasing back to 0 r/min, corresponding to a table vibration frequency from 0 Hz to 5 Hz and back to 0 Hz.

Results

Correlation between node connection and structural deformation

Both of the models M1 and M2, consist of the column frame layer and Dou-gong layer, with connections at column bases, column heads, and Dou-gong. Column bases are flat floating with 6 degrees of freedom (translation along *x*, *y*, *z* axes and rotation about the three axes). Column-head dovetail tenons are semi-rigid joints with 3 degrees of freedom (translation along *x* and *z* axes, rotation about *y* axis)⁴². Dou-gong, formed by mortise-tenon

Fig. 2 | M1 model component name and dimensions.

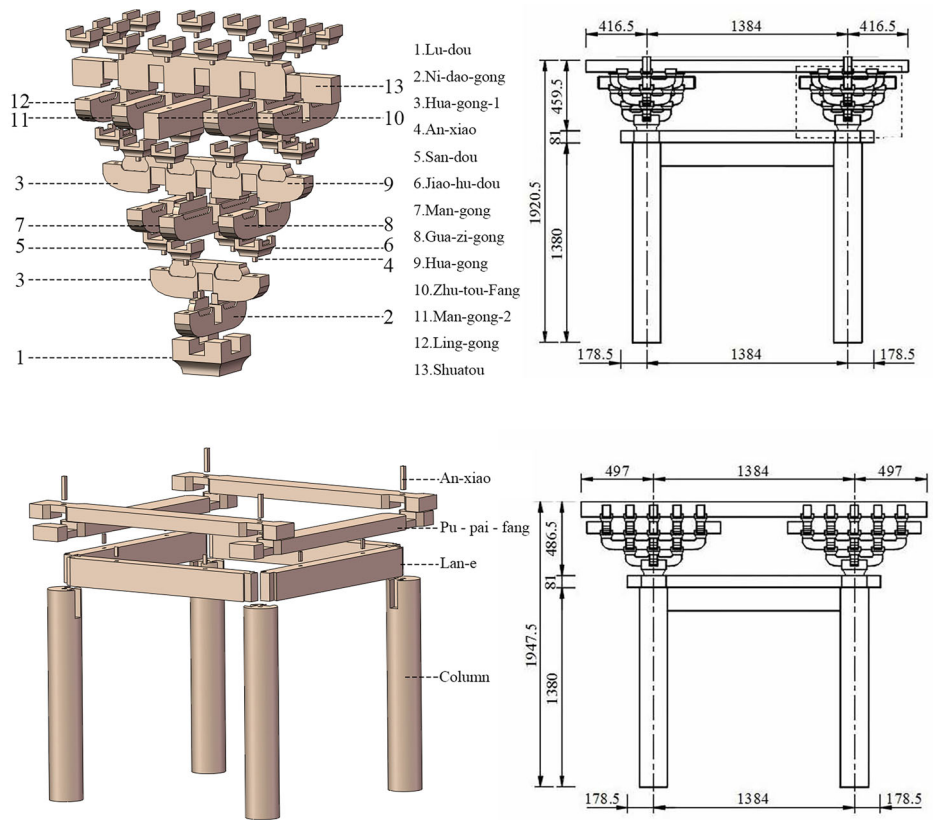


Fig. 3 | M2 model component name and dimensions.

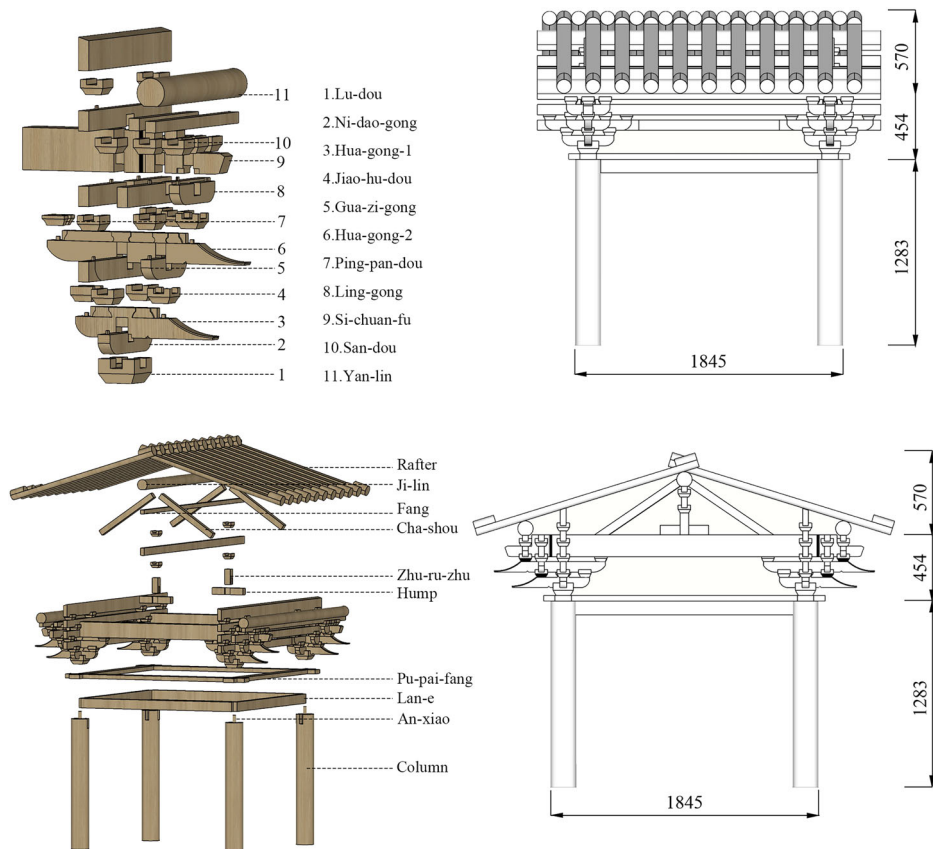


Table 1 | Wood properties for M1 and M2 models (Unit:MPa)

Model	E_L	E_T	E_R	σ_L	σ_T	σ_R
M1	8300	184	377	41	5.4	4.6
M2	8268	490	1369	64	11	7

σ compressive strength, E elastic modulus, L parallel to grain, T tangential, R radial.

lapping of multiple Dou and Gong components, plays a role in vertical and horizontal vibration reduction and energy dissipation^{43,44}, and can be simplified as multi-member hinges with stiffness and energy dissipation capacity, multi-plastic hinges, shear elastic hinges⁴⁵, or spring-damper models³⁸. Dou-gong connects Pu-pai-fang and column heads via An-xiao, with 4 degrees of freedom (rotation about x, y, z axes and translation along z axes). Its stiffness is approximately 6.5–14.3 times that of the column frame

Fig. 4 | T1 and T3 loading devices. a Perspective view of the loading device; **b** Front view of the loading device.

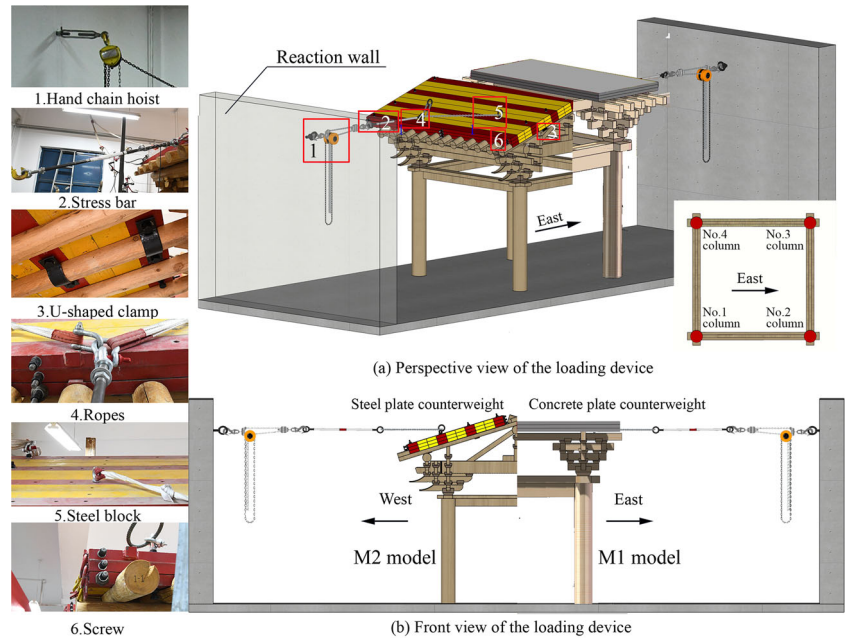


Fig. 5 | T2 and T4 loading devices. a Perspective view of the loading device; **b** Front view of the loading device; **c** Photo of the loading device.

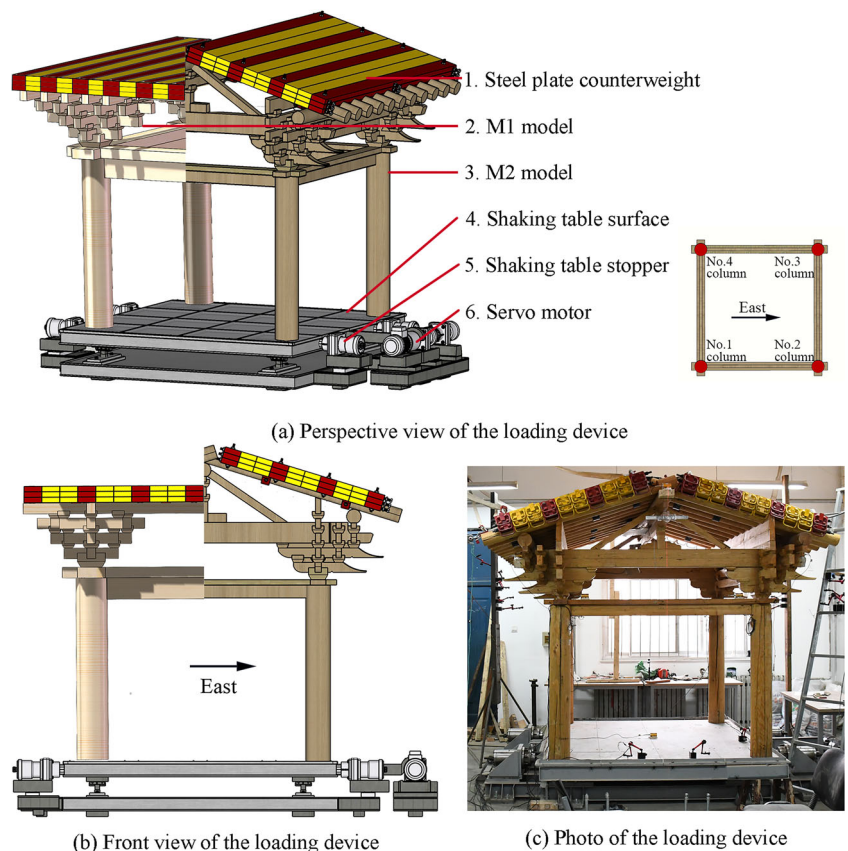


Fig. 6 | Measuring device. a M1 measuring device; **b** M2 measuring device.

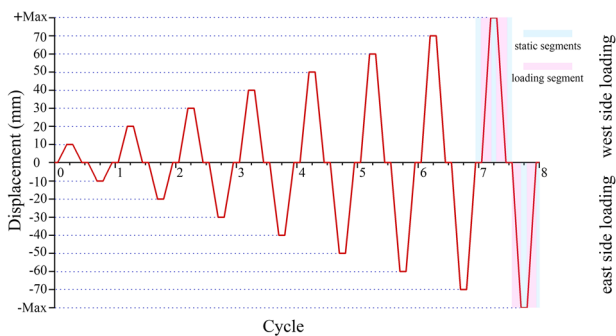
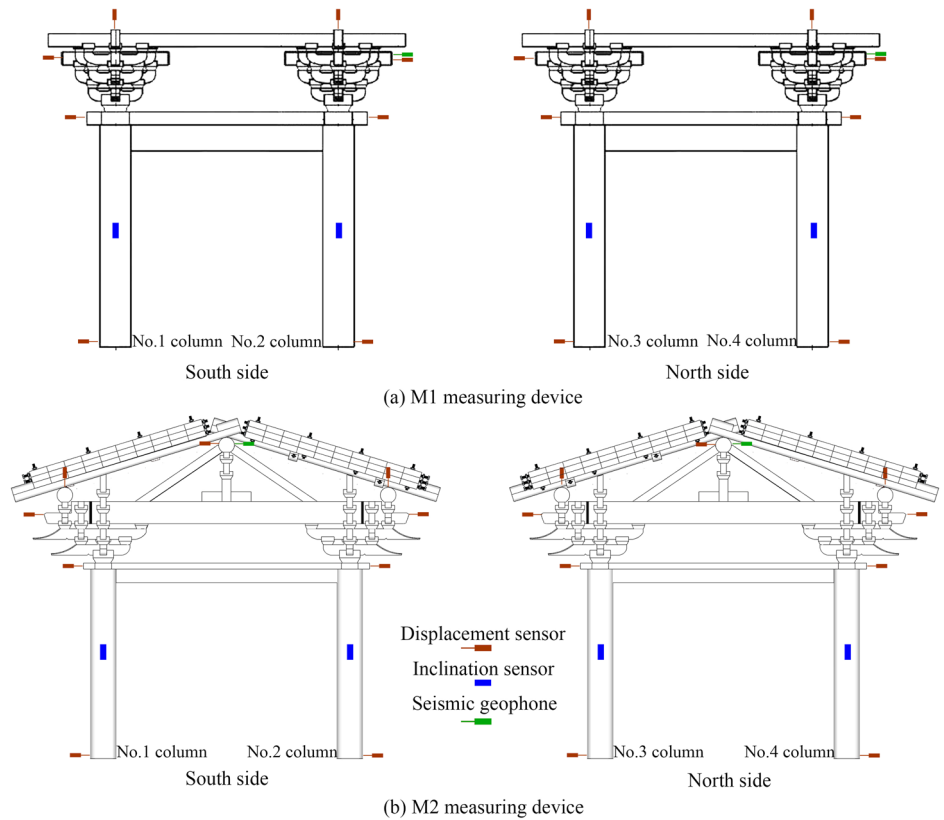


Fig. 7 | Horizontal load time history curve.

layer⁴⁶, and the diameter of the An-xiao is approximately 1/5 that of columns^{3,47}. Under increased horizontal displacement, the An-xiao are prone to plastic deformation or fracture, further weakening the connection between the Dou-gong and columns. Thus, all nodes in M1 and M2 are “weak connections”.

The overall structural deformations in the T1 and T3 tests are shown in Fig. 8a, b, respectively, with the skeleton curves shown in Fig. 8c. Both models exhibited significant rocking deformation during the quasi-static tests. At the maximum displacement, although the horizontal force did not decrease significantly, the displacement continued to increase under a nearly constant load, indicating that the structure reached a state near failure. The maximum westward displacement in T1 was 87.5 mm (89.7% of the column radius), and the eastward displacement was 84.0 mm (86.6% of the column radius). For T3, the maximum displacement in both directions was 80 mm (90% of the column radius), indicating the strong deformability of the wooden structure.

After the four tests, all the column bases showed varying degrees of slip (Fig. 9), with more significant slips in T3 and T4 (Table 2). The slip of

Column 1 in T4 reached 56% of its total radius. Additionally, all column bases exhibited lifting (Fig. 10), which was more easily observed in tests T1 and T3. At the maximum displacement, the column inclination angles in T1 and T3 ranged from 2.3° to 4.37° (Fig. 11), corresponding to inclination ratios of 1/25 to 1/13, far exceeding the allowable inclination for reinforced concrete structures (typically 1/550 of the height, with a collapse risk when exceeding 1/50). In summary, ancient Chinese wooden structures exhibit significant column slip, lifting, and inclination under both static and dynamic loading.

All four tests showed loosening of the column-head mortise-tenon joints, with deformation easily observed in T1 and T3. Under horizontal loading, the tenon pull-out and compaction states on both sides were opposite. During cyclic loading, the tenon underwent a repeated cycle of pulling out and compacting. The deformations of the column-head mortise-tenon joints at the maximum load in the final cycles of T1 and T3 are shown in Figs. 12 and 13, respectively.

In the dynamic tests T2 and T4, the maximum structural displacement response (X) and displacement magnification coefficient (β_x) directly reflected the degree of structural deformation. The β_x is calculated using Eq. 1, where X_g denotes the input displacement from the shaking table. The maximum displacement response and magnification coefficients are summarized in Table 3. It is obviously seen that the displacement response of the column frame layer was much greater than that of the other two layers, indicating its high deformability and contributing to the overall structural resilience. In contrast, the roof and Dou-gong layers demonstrated higher stiffness and greater resistance to horizontal deformation.

$$\beta_x = \frac{|X|}{|X|_g} \tag{1}$$

In summary, under seismic action, the ancient wooden structures tend to exhibit slip and uplift at the column bases, significant rocking deformation of the column frame layer, and tenon pull-out at the column heads.

Fig. 8 | Structural deformation as a whole. **a** Overall deformation of T1 structure; **b** Overall deformation of T3 structure; **c** Horizontal loading skeleton curve.

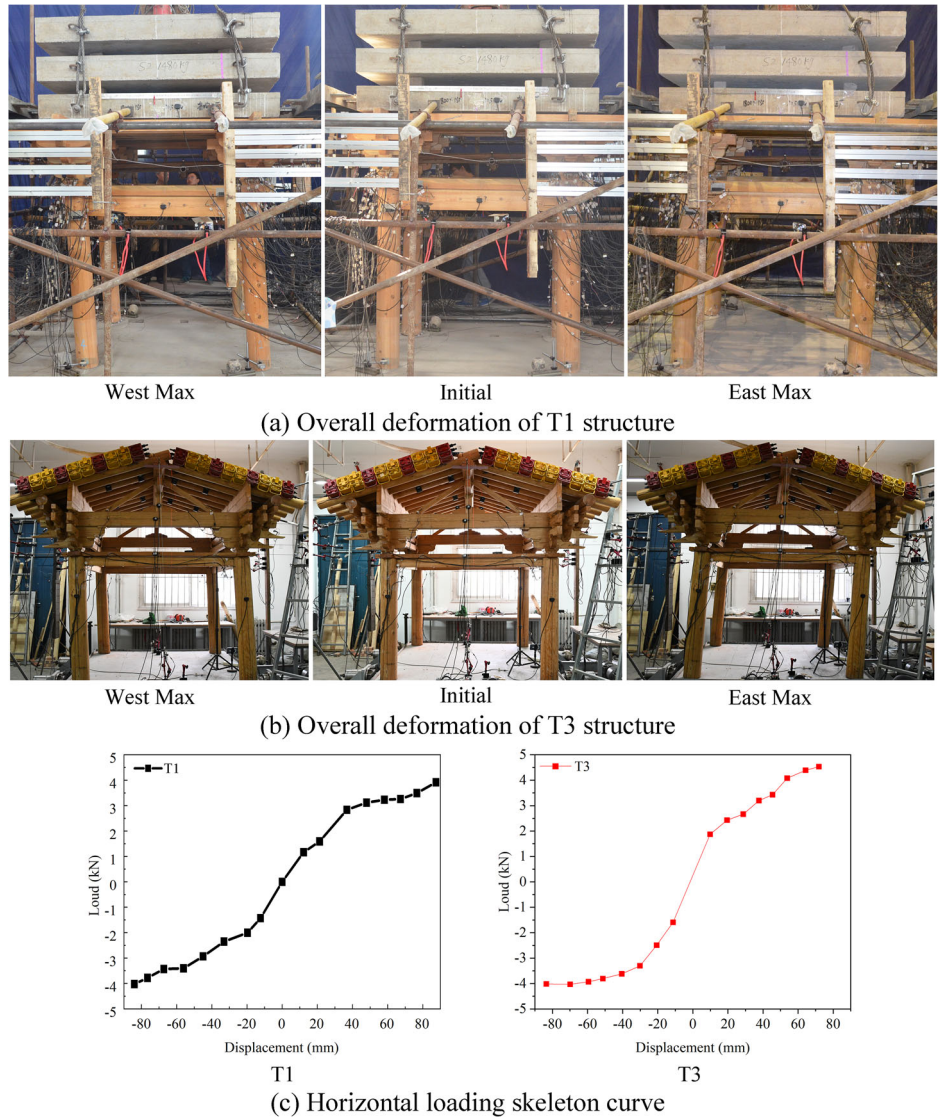


Fig. 9 | Column foot slip. **a** T3 No.1 column; **b** T3 No.3 column; **c** T4 No.1 column; **d** T4 No.2 column.

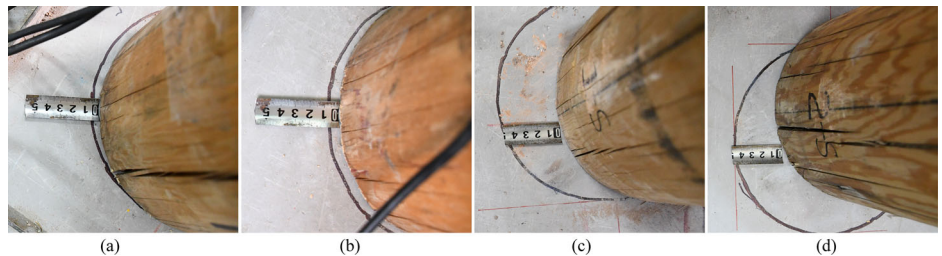


Table 2 | The base of the column slides (Unit:mm)

Test	No.1 column	No.2 column	No.3 column	No.4 column
T3	4	2	6	3
T4	50	47	28	16

However, the displacement-load curves, post-test structural stability, and component integrity all indicated good resilience of the structure. The “weak connection” characteristic of the joints provides “strong deformation” capacity, allowing the structure to avoid collapse even under large horizontal

displacements. This mechanism enables substantial structural deformation without significant damage to individual components.

Energy dissipation mechanism

Hysteresis curves can intuitively reflect the hysteretic performance of the structure, and their fullness can characterize the strength of the structure’s energy dissipation capacity. As shown in Fig. 14, the hysteresis curves of the two models obtained from the quasi-static tests are very similar, and neither curve is full. The hysteretic curves exhibit an unfull shuttle shape in the first-cycle (Fig. 14a, b) and become narrow S-shaped after the second cycle (Fig. 14c, d). Furthermore, the energy

Fig. 10 | Column base lifting. a T1 No.1 column; b T3 No.1 column; c T3 No.3 column.

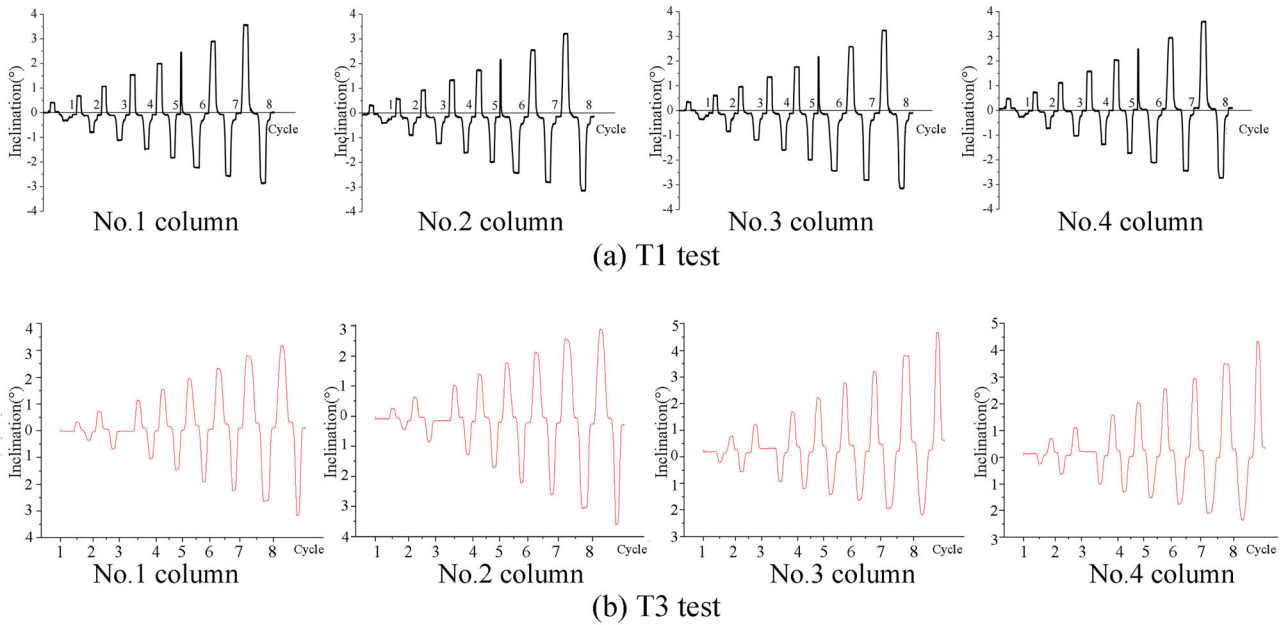
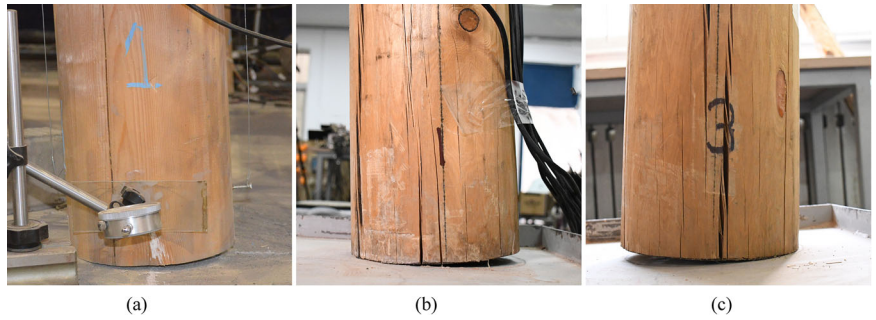


Fig. 11 | The column tilts. a T1 test; b T3 test.

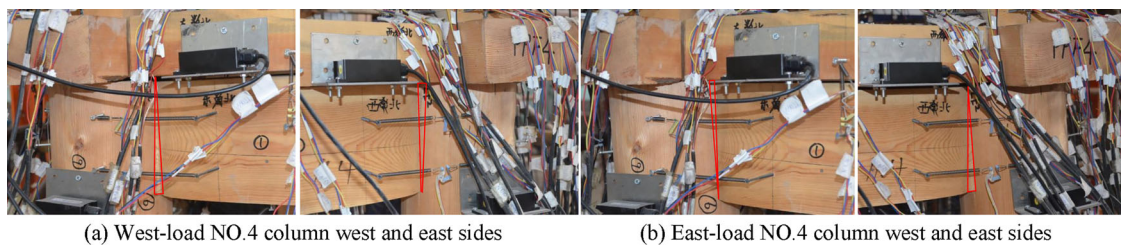


Fig. 12 | T1 mortise and tenon deformation. a West-load NO.4 column west and east sides; b East-load NO.4 column west and east sides.

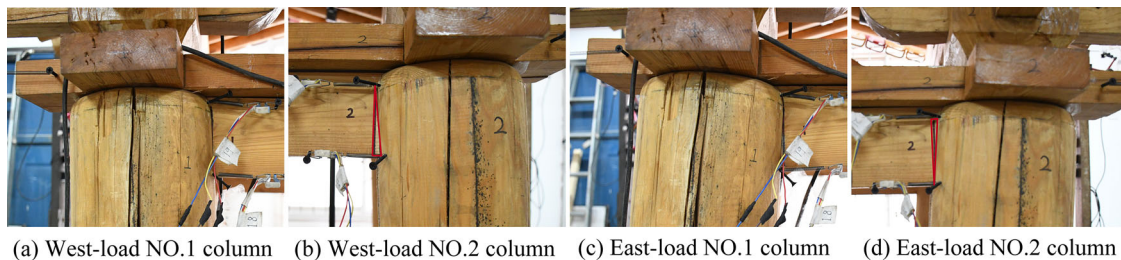


Fig. 13 | T3 mortise and tenon deformation. a West-load NO.1 column; b West-load NO.2 column; c East-load NO.1 column; d East-load NO.2 column.

Table 3 | T2 and T4 displacement magnification coefficients

Test	Location	Max displacement response	Displacement amplification factor β_x
T2	Dou-gong	38.9	6.48
	Pu-pai-fang	32.1	5.35
T4	Ji-lin	34.4	5.73
	Si-chuan-fu	33.5	5.59
	Pu-pai-fang	32.8	5.47

dissipation capacity of the structure can be quantitatively evaluated through cumulative hysteretic energy dissipation and equivalent viscous damping coefficient. The cumulative energy dissipation of T1 was 561.72 kN mm (Fig. 14e), with an equivalent viscous damping coefficient of 0.062–0.110 (Fig. 14f); while the cumulative energy dissipation of T3 was 583.04 kN mm (Fig. 14g), with a coefficient of 0.065–0.080 (Fig. 14h). These values are much lower than those obtained from the separate tests on Dou-gong⁴⁸ or beam-column joints⁴⁹. Moreover, the equivalent viscous damping coefficient of reinforced concrete frame structures with infill walls of similar span ranges from 0.2 to 0.4⁵⁰, far

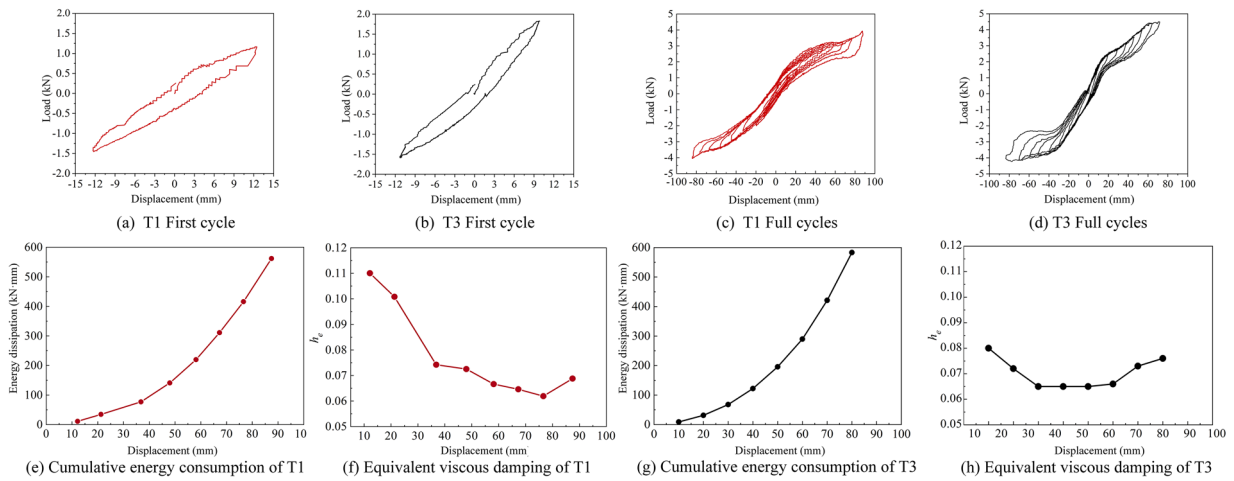
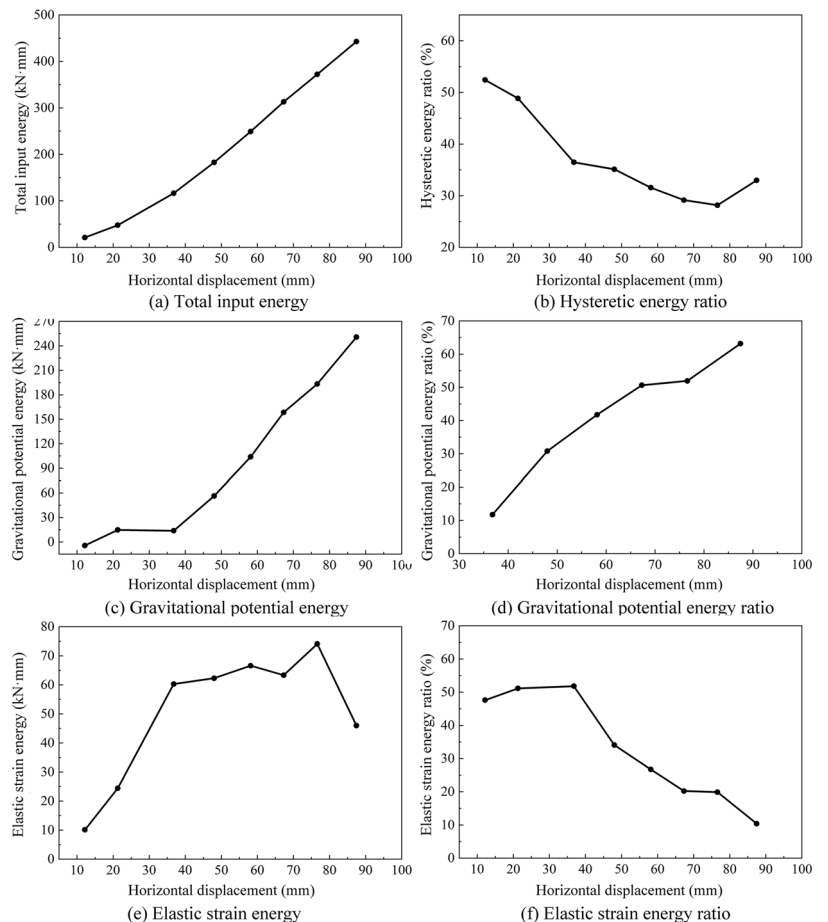


Fig. 14 | T1 and T3 hysteretic curves and energy dissipation. a T1 First cycle; **b** T3 First cycle; **c** T1 Full cycles; **d** T3 full cycles; **e** Cumulative energy consumption of T1; **f** Equivalent viscous damping of T1; **g** Cumulative energy consumption of T3; **h** Equivalent viscous damping of T3.

Fig. 15 | T1 input energy and proportion. a Total input energy; **b** Hysteretic energy ratio; **c** Gravitational potential energy; **d** Gravitational potential energy ratio; **e** Elastic strain energy; **f** Elastic strain energy ratio.



higher than that of wooden structures. The above indicates that the energy dissipation capacity of such timber structure is weak.

It is obvious that energy dissipation is not the primary way for the ancient timber structures to resist earthquakes; however, the rocking deformation endows it with a special energy conversion mechanism, which plays a key role in the seismic resistance. The energy balance equation for wooden frames in quasi-static tests is shown in Eq. 2⁵¹, where E_I is the total energy input by horizontal external loads; E_H is the energy dissipated through friction and plastic deformation between wooden components (hysteretic energy dissipation); E_G is the gravitational potential energy stored owing to vertical lifting; and E_E is the elastic strain energy stored in the elastic deformation of wooden components.

$$E_I = E_H + E_E + E_G \quad (2)$$

Table 4 | Ductility coefficient

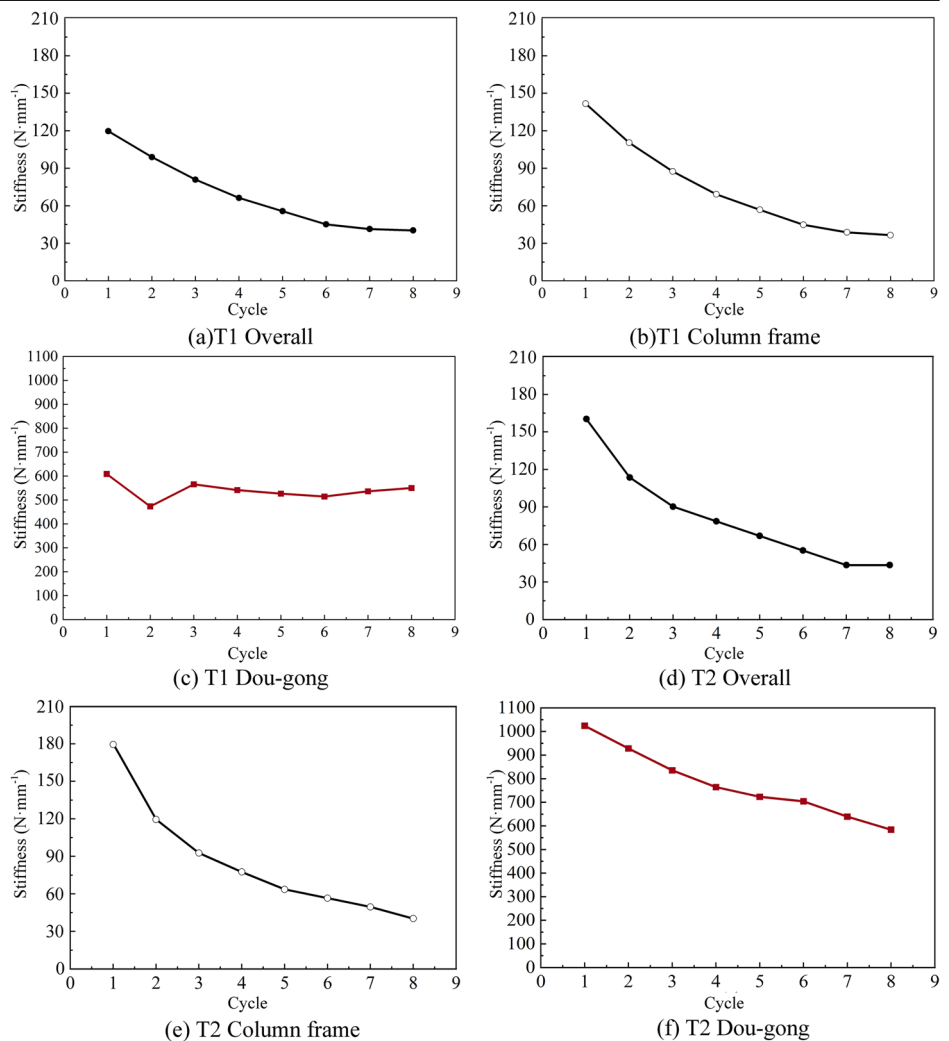
Test	Yield point (mm)	Extreme point (mm)	Ductility coefficient
T1	21.5	85.8	3.99
T3	12.8	80.0	6.27
RC	-	-	3.37-4.16 ^{52,53}
Steel structure	-	-	1.68-3.67 ⁵⁴
Masonry structure	-	-	2.04-4.24 ⁵⁵

The total energy input to the wooden frame in T1 is shown in Fig. 15a, and the proportion of hysteretic energy dissipation in the total input energy is illustrated in Fig. 15b. The hysteretic energy dissipation accounted for 52% in the first cycle of T1, decreasing significantly with increasing horizontal displacement to 33% in the eighth cycle. This indicates that when the horizontal displacement amplitude is small, the structure dissipates more energy through hysteresis. After the fifth cycle, hysteretic energy dissipation was no longer the main method for resisting earthquakes.

The gravitational potential energy calculated from the average vertical displacement in T1 is shown in Fig. 15c, and its proportion of the total input energy is shown in Fig. 15d. The gravitational potential energy accounts for a negligible proportion in the first two cycles. With increasing horizontal displacement, vertical lifting of the wooden frame became significant, and gravitational potential energy increased linearly, accounting for 57% of the total energy dissipation in the eighth cycle. This indicates that under horizontal earthquake action, column frame layer rocking causes vertical lifting of the roof, converting seismic input energy into gravitational potential energy stored in the wooden structure and significantly reducing component damage. This energy conversion mechanism is key to the ability of traditional wooden structures to resist multiple earthquakes (especially strong ones) and explains their weak energy dissipation but strong seismic performance.

The elastic strain energy, calculated by subtracting the hysteretic energy dissipation and gravitational potential energy from the total input energy, is shown in Fig. 15e, while its proportion to the total input

Fig. 16 | Stiffness coefficient. a T1 Overall; b T1 Column frame; c T1 Dou-gong; d T2 Overall; e T2 Column frame; f T2 Dou-gong.



energy is presented in Fig. 15f. From cycle 1–3, the elastic strain energy increased significantly and accounted for more than 50% of the total energy input in each of these three cycles. After the third cycle, the elastic strain energy barely increased any further. However, due to the continuous growth of the total energy input, the proportion of elastic strain energy decreased markedly, dropping to 10% in the final cycle.

Displacement ductility refers to the ability of a structure to withstand deformation without a significant loss of load-bearing capacity, which can be quantified using the displacement ductility coefficient. A higher coefficient indicates stronger deformability and higher seismic resistance. The ductility coefficients of T1 and T3 and other typical structures are listed in Table 4, in which the yield point refers to the point on the skeleton curve where there is an obvious deviation from linearity. By comparing the ductility coefficient of other structures, it is shown that the timber structure has strong ductility and good bearing capacity under large deformation.

In summary, the unfull hysteretic curve, low cumulative energy dissipation, and low equivalent viscous damping coefficient all indicate weak energy dissipation capacity in the ancient wooden structure. However, through its rocking behavior and gravitational potential energy conversion mechanism, the structure exhibits excellent ductility. As a result, the ancient timber structure demonstrates structural characteristics of low energy dissipation coupled with strong seismic resistance, a feature that effectively minimizes damage to the wooden components during earthquakes.

Table 5 | Stiffness of each structural layer (N · mm⁻¹)

Test	Overall beam frame	Column frame layer	Dou-gong layer
T1	49–117	53–143	473–609
T3	60–160	60–180	723–1024

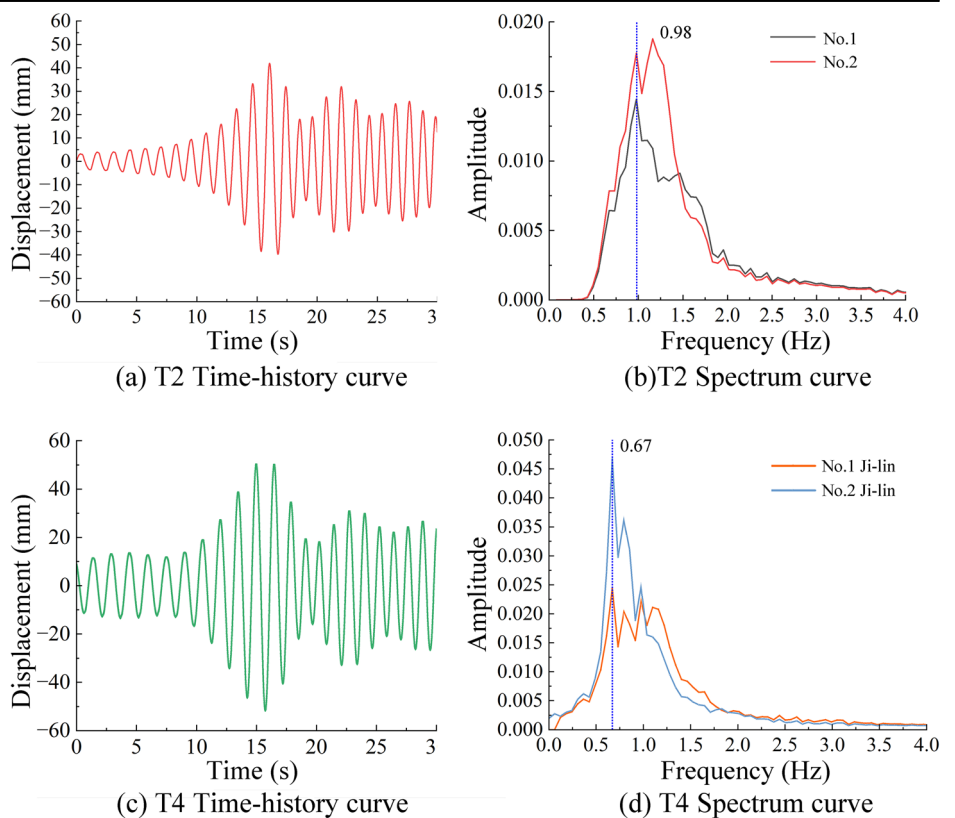
Dynamic characteristics of the structure

The resonance frequency refers to the characteristic frequency at which a structure exhibits a significantly amplified amplitude owing to the coincidence of its natural frequency with the frequency of external dynamic excitation. When the resonance occurs, a large amount of energy accumulates in the structure, potentially leading to excessive vibrations or damage. The natural frequency of a structure is determined by its mass, stiffness, and damping properties. Under normal circumstances, when the mass and damping are constant, the structural frequency increases as the stiffness increases.

The stiffness of the overall structure, column frame layer, and Dou-gong layer is calculated using the displacement-load relationships obtained from tests T1 and T3. As shown in Fig. 16 and Table 5, the stiffness of the column frame layer is slightly greater than that of the overall structure, and both exhibit a consistent decreasing trend with increasing horizontal displacement amplitude. The stiffness of the Dou-gong layer is approximately 8–12 times that of the column frame layer. Due to significant differences in horizontal stiffness between layers, the natural frequencies of each structural layer differ substantially. Thus, during an earthquake, the column frame layer and Dou-gong layer do not resonate simultaneously, significantly reducing the overall resonance effects and mitigating the acceleration.

The displacement time-history and spectrum curves obtained from T2 and T4 are shown in Fig. 17. It can be observed that although the amplitude input by the shaking table remains constant, the displacement response of the structure significantly changes with variations in the input frequency. In both the T2 and T4 tests, the displacement response of the structure reaches its maximum at a specific input frequency, which is close to the natural frequency of the structure, resulting in a resonance effect. According to the test results, the resonant frequency of the structure in the T2 test is 0.98 Hz, with a maximum displacement response of 38.9 mm, while in the T4 test, the resonant frequency is 0.67 Hz, with a maximum displacement response of 34.4 mm. The maximum displacement response of the structure in both

Fig. 17 | Time history curve and spectrum curve. a T2 Time-history curve; b T2 Spectrum curve; c T4 Time-history curve; d T4 Spectrum curve.



tests is only 1/5 of the column diameter, which is far from reaching the ultimate displacement of the structure. This is primarily due to the significant difference in stiffness between the column frame layer and the Dou-gong layer as analyzed above, which prevents simultaneous resonance of the structural layers, thereby reducing the overall structural response. Additionally, due to the lower stiffness of the column frame layer, vibrations at higher frequencies are difficult to transmit through the column frame layer to the layers above it. Therefore, under higher frequency excitation (input frequency exceeding 2 Hz), the responses of both the column frame layer and the Dou-gong layer are relatively small.

The ancient wooden structures exhibit functions analogous to modern seismic isolation and energy-dissipating structures. The low-stiffness column frame layer acts as an isolation layer, blocking the transmission of high-frequency vibrations to the upper layers. The Dou-gong layer performs the function of energy-dissipating, reducing vibrations of the structure via inter-component friction. Synergistic work between layers enables the superior seismic performance characterized by “weak resonance, strong synergy”.

Discussion

(1) Connections in ancient wooden structures, such as flat floating column bases, column-head mortise-tenon joints, and Dou-gong joints, all possess more than three degrees of freedom and are prone to deformation. During mechanical testing, the column bases exhibit obvious slipping and lifting, while the mortise-tenon joints experience noticeable pull-out deformation. Despite these localized deformations, the overall structure can achieve a maximum horizontal displacement of up to 90% of the column radius, with a maximum rotation angle of 5.36°, far exceeding the deformation limits allowed in modern structures. Thus, the ancient wooden structures demonstrate a unique characteristic of “weak connections yet strong deformability”.

(2) The hysteresis curves of the ancient timber structure obtained from the quasi-static tests are highly unfull, with an equivalent viscous damping coefficient ranging only from 0.061 to 0.110, indicating relatively low energy dissipation capacity. However, the rocking behavior of the structure provides a distinct energy conversion mechanism. During horizontal deformation, vertical uplift transforms a portion of the input energy into gravitational potential energy, which is stored within the structure. This converted energy can account for over 50% of the total input energy. As a result, the structure exhibits favorable ductility and significantly reduced earthquake-induced damage to its components, demonstrating a characteristic of “weak energy dissipation yet strong earthquake resistance”.

(3) The column-frame layer and the Dou-gong layer exhibit significant differences in stiffness, and under dynamic excitation, these two layers are not susceptible to synchronous resonance. Consequently, the displacement response of the overall structure remains within a safe range even when the external excitation frequency approaches the natural frequency of the structure. Furthermore, the various layers demonstrate an effective collaborative working mechanism under dynamic excitation. The more flexible column-frame layer serves as an isolation system, effectively inhibiting the transmission of high-frequency vibrations to the upper layers. Simultaneously, the Dou-gong layer contributes to energy dissipation and vibration damping through friction and compression among its numerous components. This mechanism of “weak resonance yet strong synergy” enhances the structural resilience during seismic events.

In summary, the semi-rigid mortise-tenon joints, differentiated structural layer combinations, and the inherent properties of wood collectively contribute to the “three strong and three weak” characteristics of ancient Chinese wooden structures. This study reveals the scientific essence of ancient earthquake-resistant wisdom through structural mechanical tests, demonstrating the organic balance of wooden structures optimized through empirical practices despite material limitations. This research mainly focuses on the mechanical organic of three important column-frame joints. However, the organic of ancient timber structures is also reflected in the

more detailed structure and the use of materials, which needs to be further studied. Those studies not only deepen understanding of traditional construction techniques but also provide new insights for developing sustainable, low-damage seismic systems.

Data availability

All data generated or analyzed during this study are available from the corresponding author upon reasonable request.

Received: 7 August 2025; Accepted: 11 December 2025;

Published online: 31 December 2025

References

- Liang, S. C. Notes on the architecture of Foguang Temple in Wutai Mountain. *J. J. China Constr. Soc.* **7**, 14 (1944).
- Liang, S. C. *Annotations on Yingzao Fashi* (Tsinghua University Press, 2006).
- Chai, Z. J. *Report on the Restoration Project of Shengmu Hall in Jinci Taiyuan* (Cultural Relics Press, 2000).
- Wang, Y. Z. & Xu, Y. T. Study on the “large scale” and scale composition in Liao dynasty architectural construction: a case study of Liao Structures in Dule Temple, Fengguo Temple, and Kaishan Temple. *J. Palace Mus.* 24–47+150 (2023).
- Zhang, S. Q. Discussion on the benchmark timber in the timber work system of Yingzao Fashi. *J. Archit. Hist.* 73–81 (2016).
- Zhang, C. Y. Study on mechanical properties and conservation restoration of dougong in Shengmu Hall of Jinci. *D. Taiyuan Taiyuan Univ. Technol.* 139–140 (2022).
- Du, Q. M. On the design module of large timber work in Song dynasty’s yingzao fashi. *J. Technol. Anc. Archit. Gard.* 39–47 (1999).
- Wang, S. Q., Xie, Z. W. & Zhou, Y. L. Analysis on the evolution of timber frames in tusi architecture based on yingzao fashi: a case study of zushi hall in Laosi City. *J. Zhuangshi* 127–129 (2023).
- Xu, Y. T. Study on the controlling scale rules of large timber work in Yingzao Fashi. *J. Palace Mus.* 36–44+157–158 (2015).
- Liang, S. C. *A Pictorial History of Chinese Architecture* (Baihua Literature and Art Publishing House, 2001).
- Ma, B. J. *Timber Construction Techniques of Ancient Chinese Architecture* (Science Press, 2003).
- Liang, S. C. *Illustrated Explanation of the Engineering Rules of the Qing Ministry of Works* (Tsinghua University Press, 2006).
- Zhang, B. Z., Song, X. B., Lu, Y. & Chen, X. J. 2024. Seismic performance of Li-Tie type brick masonry infilled wooden frames considering joint damage: degradation mechanism and hysteretic model. *J. Soil Dyn. Earthq. Eng.* **187**, 109008 (2024).
- Li, J. & Yingzao F. M. *Shanghai* (Commercial Press, 1954).
- Zhang, L., Liu, C. & Zhou, T. Experimental study on mechanical properties of column foot of ancient timber structures - take the drum-shaped plinth as an example. *J. Struct.* **40**, 1002–1013 (2022).
- Zhang, B. Z., Xie, Q. F., Li, S. Y., Zhang, L. P. & Wu, Y. J. Effects of gaps on the rotational performance of traditional straight mortise-tenon joints. *J. Eng. Struct.* **260**, 114231 (2022).
- Zhang, B. Z., Xie, Q. F., Hu, J. F., Zhang, L. P. & Wu, Y. J. Rotational performance of traditional straight mortise-tenon joints with gap: theoretical model and numerical analyses. *J. Int. J. Archit. Herit.* **17**, 1701–1718 (2023).
- Ilgın, H. E., Pajunen, S., Leivo, V. & Karjalainen, M. Structural performance of a novel dovetailed timber panel subjected to out-of-plane bending. *J. Case Stud. Constr. Mater.* **23**, e05095 (2025).
- Zhang, B. Z., Song, X. B., Xie, Q. F. & Xue, J. Y. Seismic behavior of looseness-induced inclined mortise and tenon joints in ancient timber structures: experimental tests, multi-scale finite element model, and behavior degradation. *J. Eng. Struct.* **318**, 118–680 (2024).

20. Li, S. C., Chen, L. K., Jiang, L. Z. & Li, J. Q. Experimental investigation on the seismic behavior of the semi-rigid one-way straight mortise-tenon joint of a historical timber building. *J. Int. J. Archit. Herit.* **14**, 1135–1147 (2020).
21. Chen, Z. Y., Zhu, E. C., Lam, F. & Pan, J. L. Structural performance of Dou-Gong brackets of Yingxian Wood Pagoda under vertical load-an experimental study. *J. Eng. Struct.* **80**, 274–288 (2014).
22. Kim, Y. M. Evaluation of structural performance of multi-tiered roof Korean traditional timber building Daeungbojeon Hall of Magoksa Temple under vertical load. *J. Comput. Struct. Eng. Inst. Korea* **37**, 17–24 (2024).
23. Nimwegen, S. E., Goosse, J. & Latteur, P. Opportunities and limitations of robotically-shaped subtractive fabrication structural timber connections for multi-level log frame buildings. *J. Build. Eng.* **112**, 113917 (2025).
24. Han, X. L. Effect of column foot tenon on behavior of larch column base joints based on concrete plinth. *J. Bio. Res.* **15**, 6648–6667 (2020).
25. Meng, X. J., Yang, Q. S., Wei, J. W. & Li, T. Y. Experimental investigation on the lateral structural performance of a traditional Chinese pre-Ming dynasty timber structure based on half-scale pseudo-static tests. *J. Eng. Struct.* **167**, 582–591 (2018).
26. Zhang, B. Z., Xie, Q. F. & Li, S. Y. Numerical analysis of traditional Chinese timber structure: simplified finite element model and composite elements of joints. *J. J. Build. Eng.* **67**, 106027 (2023).
27. Zhang, B. Z., Song, X. B., Xie, Q. F. & Xue, J. Y. Seismic behavior of damaged ancient timber buildings: multi-scale finite element model, performance degradation, and experimental verification. *J. Earthq. Eng.* **29**, 709–733 (2025).
28. Meng, X. J., Li, T. Y., Yang, Q. S. & Wei, J. W. Seismic mechanism analysis of a traditional Chinese timber structure based on quasi-static tests. *J. Struct. Control Health Monit.* **25**, e2245 (2018).
29. Kuang, Y. Y. Stiffness analysis of typical mortise-tenon joints in timber buildings. *J. Build. Struct.* **50**, 113–116 (2020).
30. Chen, J. Y., Li, T. Y., Yang, Q. S., Shi, X. W. & Zhao, Y. X. Degradation laws of hysteretic behaviour for historical timber buildings based on pseudo-static tests. *J. Eng. Struct.* **156**, 480–489 (2018).
31. Sha, B., Xie, L. L., Yong, X. Q. & Li, A. Q. Hysteretic behavior of an ancient Chinese multi-layer timber substructure: a full-scale experimental test and analytical model. *J. Build. Eng.* **43**, 103–163 (2021).
32. Meng, Y. & Chen, W. How timber was used in ancient Chinese timber building construction. *J. Archit.* 41–45 (2019).
33. Can Altunışık, A., Sunca, F. & Sevim, B. Modal parameter identification and seismic assessment of historical timber structures under near-fault and far-fault ground motions. *J. Struct.* **47**, 1624–1651 (2023).
34. Qi, Y. & Lin, Y. Study on architectural characteristics and construction logic of Dacheng Hall in Confucian temples in Shaanxi region during the Ming dynasty. *J. Archit.* 109–113 (2023).
35. Wang, N. Rules and proportions: analysis of the composition proportions of the east main hall of Foguang Temple in Wutai Mountain. *J. Archit.* 29–36 (2017).
36. Cai, N., Wu, G. Y., Li, L. B. & Sun, P. Connotation of traditional timber building design revealed by Xiandian Hall of Huayang Temple in Guanzhong. *J. Archit.* **951**, 109–115 (2023).
37. Liu, Y. From material properties and concepts: experiences in timber structure construction practice. *J. Archit.* 79–83, 110619 (2023).
38. Tachibana, K. Shake table test of a full-scale ten-story mass timber building designed with Japanese building standard law. *J. Eng. Struct.* **343**, 120851 (2025).
39. Zhang, C. Y., Gao, Y. B. & Duan, E. Z. Calculation and analysis of the loads of dou-gong brackets on ming dynasty wooden buildings in China. *J. Teh. Vjesn. Tech. Gaz.* **27**, 1638–1647 (2020).
40. Chen, J. Y. Dead load of song-style timber roofs and similarity relationship of timber module system. *J. Civ. Archit. Environ. Eng.* **38**, 27–33 (2016).
41. Maeda, T. Column rocking behavior of traditional wooden buildings in Japan. C. Proc. 10th World Conf. Timber Eng. Miyazaki, 2008.
42. Li, Y. H., Deng, Y. & Aigun, Li. Simplified simulation method for hysteretic behavior of wood brackets. *J. Perform. Constr. Facil.* **35**, 04021085 (2021).
43. Zhang, X. C., Xue, J. Y., Zhao, H. T. & Sui, Y. Experimental study on Chinese ancient timber-frame building by shaking table test. *J. Struct. Eng. Mech.* **40**, 453–469 (2011).
44. Chu, C. H., Liao, C. J. & Lin, S. C. Comparing augmented reality-assisted assembly functions—a case study on dougong structure. *J. Appl. Sci. Basel.* **10**, 3383 (2020).
45. Yang, Z. X. et al. Seismic vulnerability assessment of historical timber temples: a case study of the Hanging Temple in China. *J. Res. Sq.* **13**, 4 (2024).
46. Sha, B. et al. An experimental study of the combined hysteretic behavior of dougong and upper frame in Yingxian Wood Pagoda. *J. Constr. Build. Mater.* **305**, 124723 (2021).
47. Liang, S. C. *Qing-Style Construction Regulations* (Tsinghua University Press, 2006).
48. Gao, D. F., Li, F., Liu, J., Deng, H. X. & Yang, Y. Experimental study on seismic performance of dou-gong structural layers in ancient timber buildings. *J. Earthq. Eng. Eng. Vib.* **34**, 131–139 (2014).
49. Li, X. W., Zhao, J. H., Ma, G. W. & Chen, W. Experimental study on the seismic performance of a double-span traditional timber frame. *J. Eng. Struct.* **98**, 141–150 (2015).
50. Feng, Y. Experimental study on seismic performance of reinforced concrete frames with vertical slit concrete infill walls. *J. Build. Struct.* **50**, 71–76 (2020).
51. Meng, X. J. *Study on Seismic Performance and Seismic Mechanism of Song-Style Traditional Timber Structures* (Taiyuan University of Technology, 2019).
52. Ma, J. X., Ma, Y. & Jiang, J. N. Experimental study on seismic behavior of corroded RC rectangular columns strengthened with CFRP sheets. *J. Vib. Shock.* **44**, 298–310 (2025).
53. Xiong, X. L., Hu, P. & Zhao, Z. H. Seismic behavior analysis of long-span steel reinforced concrete beam-column oblique angle joints. *J. Shenyang Jianzhu Univ.* **41**, 473–484 (2025).
54. Zou, Y., Miao, J. W. & Wang, C. Q. Experimental study on seismic behavior of corrugated steel plate composite frame joints. *J. Build. Struct.* **53**, 136–140+118 (2023).
55. Li, S. C. & Li, S. C. Seismic behavior of energy-saving block composite wall with concealed multi-frame after double-sided fire. *J. Eng. Mech.* 1–18 (2025).
56. Chen, Z. Y. Study on mechanical properties of typical joints and structures of Yingxian wood pagoda. *D. Harbin Harbin Instit. Technol.* 163-165 (2011).
57. Meng, X. J., Li, T. Y. & Yang, Q. S. Lateral structural performance of column frame layer and dou-gong layer in a timber structure. *J. KSCE J. Civ. Eng.* **23**, 666–677 (2019).

Acknowledgements

This research was supported by the National Key Research and Development Program Fund (2023YFF0906300), the Humanities and Social Sciences Research Project of the Ministry of Education (23YJC760151), the National Natural Science Foundation of China (52108465), the Basic Research Program of Shanxi province (202403021212329).

Author contributions

Z.C.Y. conducted static loading test while analysed the related data and drafted the original manuscript. M.X.J. conducted dynamic loading test while analysed the related data and revised the manuscript. W.Y. drawn the

diagrams for the paper. J.Z.R. undertook the site investigations and collected the data. W.S.Q. performed field experiments. All authors read and approved of the final manuscript.

Competing interests

The authors declare no competing interests.

Additional information

Correspondence and requests for materials should be addressed to Xianjie Meng.

Reprints and permissions information is available at <http://www.nature.com/reprints>

Publisher's note Springer Nature remains neutral with regard to jurisdictional claims in published maps and institutional affiliations.

Open Access This article is licensed under a Creative Commons Attribution-NonCommercial-NoDerivatives 4.0 International License, which permits any non-commercial use, sharing, distribution and reproduction in any medium or format, as long as you give appropriate credit to the original author(s) and the source, provide a link to the Creative Commons licence, and indicate if you modified the licensed material. You do not have permission under this licence to share adapted material derived from this article or parts of it. The images or other third party material in this article are included in the article's Creative Commons licence, unless indicated otherwise in a credit line to the material. If material is not included in the article's Creative Commons licence and your intended use is not permitted by statutory regulation or exceeds the permitted use, you will need to obtain permission directly from the copyright holder. To view a copy of this licence, visit <http://creativecommons.org/licenses/by-nc-nd/4.0/>.

© The Author(s) 2025